Biochimica et Biophysica Acta 1827 (2013) 817–825

Contents lists available at SciVerse ScienceDirect

Biochimica et Biophysica Acta

journal homepage: www.elsevier.com/locate/bbabio

Modulation of ceramide-induced cell death and superoxide production by mitochondrial DNA-encoded respiratory chain defects in *Rattus* xenocybrid mouse cells

Ian A. Trounce [a,1,*], Peter J. Crouch [b,c,1], Kirstyn T. Carey [d], Matthew McKenzie [d]

[a] Centre for Eye Research Australia, Department of Ophthalmology, University of Melbourne, Royal Victorian Eye and Ear Hospital, East Melbourne, Victoria 3002, Australia
[b] Department of Pathology, The University of Melbourne, Victoria 3010, Australia
[c] The Florey Institute for Neuroscience and Mental Health, The University of Melbourne, Victoria 3010, Australia
[d] Centre for Reproduction and Development, Monash Institute of Medical Research, Monash University, Victoria 3168, Australia

ARTICLE INFO

Article history:
Received 22 January 2013
Received in revised form 26 March 2013
Accepted 28 March 2013
Available online 6 April 2013

Keywords:
Oxidative phosphorylation
Reactive oxygen species
Mitochondrial DNA
Ceramide
Mouse fibroblast
Mitochondrial disease

ABSTRACT

Mitochondria play an integral role in cell death signaling, yet how mitochondrial defects disrupt this important function is not well understood. We have used a mouse L-cell fibroblast model harboring *Rattus norvegicus* mtDNA (Rn xenocybrids) to examine the effects of multiple oxidative phosphorylation (OXPHOS) defects on reactive oxygen species (ROS) generation and cell death signaling. Blue native-PAGE analyses of Rn xenocybrids revealed defects in OXPHOS complex biogenesis with reduced steady-state levels of complexes I, III and IV. Isolated Rn xenocybrid mitochondria exhibited deficiencies in complex II + III and III activities, with CIII-stimulated ROS generation 66% higher than in control mitochondria. Rn xenocybrid cells were resistant to staurosporine-induced cell death, but exhibited a four-fold increase in sensitivity to ceramide-induced cell death that was caspase-3 independent and did not induce chromosomal DNA degradation. Furthermore, ceramide directly inhibited Rn xenocybrid complex II + III activity by 97%, although this inhibition could be completely abolished by exogenous decylubiquinone. Ceramide also induced a further increase in ROS output from Rn xenocybrid complex III by 42%. These results suggest that the interaction of ceramide with OXPHOS complex III is significantly enhanced by the presence of the xenotypic *Rattus* cytochrome *b* in complex III, likely due to the increased affinity for ceramide at the ubiquinone binding site. We propose a novel mechanism of altered mitochondrial cell death signaling due to mtDNA mutations whereby ceramide directly induces OXPHOS complex ROS generation to initiate cell death pathways.

1. Introduction

Much of a cell's energy requirements are met by the mitochondria, organelles which can oxidize sugars, fats and amino acids to generate ATP. This metabolic process, termed oxidative phosphorylation (OXPHOS), is performed by a series of five enzyme complexes within the mitochondrial inner membrane. These complexes contain multiple protein subunits, encoded by both the nuclear genome and the mitochondria's own DNA (mtDNA), which must be assembled together in a coordinated fashion to form the mature holocomplexes. Mutations in either nuclear or mtDNA can cause OXPHOS complex deficiencies, resulting in metabolic disorders that affect approximately 1 in 5000 live births [1,2]. These disorders encompass a wide variety of multisystemic degenerative diseases, commonly referred to as mitochondrial encephalomyopathies, which can exhibit various combinations of clinical features. Brain and muscle are usually affected, although other tissues that have high energy requirements may also be involved.

Although biochemical defects have been associated with various mtDNA mutations, secondary effects, such as elevated ROS production, may also modulate the primary OXPHOS deficiency. For example, the *MTND1* and *MTND6* mutations associated with Leber Hereditary Optic Neuropathy (LHON) [3,4] alter the binding of CoQ_{10} to complex I, resulting in increased levels of ubisemiquinone and ROS generation which in turn may contribute to the premature death of the optic nerve [5]. Increased ROS generation has also been observed in differentiated NT2 neurons containing *MTND4* or *MTND1* LHON mutations [6] with a concomitant increase in sensitivity to Fas-induced apoptosis [7]. Other mtDNA mutations, such as a 4 bp deletion in the cytochrome *b* gene associated with complex III deficiency in a patient with Parkinsonism, are also associated with increased ROS generation [8]. These results suggest that elevated ROS levels, due to mtDNA mutation-induced OXPHOS defects, contribute to disease pathology.

Abbreviations: mtDNA, mitochondrial DNA; OXPHOS, oxidative phosphorylation; ROS, reactive oxygen species; DCFH, 2′,7′-dichlorodihydrofluoroscein; Rn, *Rattus norvegicus*; BN-PAGE, Blue native polyacrylamide gel electrophoresis

* Corresponding author at: Centre for Eye Research Australia, Royal Victorian Eye and Ear Hospital, 32 Gisborne Street, East Melbourne, Victoria 3002, Australia. Tel.: +61 3 99298160; fax: +61 3 99298164.
E-mail address: i.trounce@unimelb.edu.au (I.A. Trounce).

[1] These authors contributed equally.

0005-2728/$ – see front matter © 2013 Elsevier B.V. All rights reserved.
http://dx.doi.org/10.1016/j.bbabio.2013.03.012

However, contrary to these findings, the accelerated aging phenotype in the 'mtDNA mutator' mouse (which has high levels of mtDNA mutations and deletions due to a knock-in mutation in the PolgA gene) is not associated with increased ROS generation [9].

One important molecule that has been implicated in ROS-linked cell-death signaling is ceramide, a lipid produced by either *de novo* synthesis or from the breakdown of sphingomyelin after activation of sphingomyelinase (which is classically induced by the TNFα death receptor [10]). Cell permeant ceramide analogs (C_2 and C_6) have been shown to induce cell death that exhibits either apoptotic or necrotic features depending on cell type [11–14] and to increase mitochondrial ROS production during cell death [15–18]. NADH- and FADH-linked respiration of rat heart mitochondria is inhibited by C_2- and C_6-ceramide, with ceramide also directly inhibiting complex I and III enzymatic activity [16,19–21].

Although the effects of ceramide are well known, ceramide-induced cell death signaling consequent to mtDNA mutations has not been investigated. To examine these effects, in vitro and in vivo mouse models of mtDNA disease would be highly beneficial. However, the unique features of mitochondrial genetics, including the high cellular mtDNA copy number and the lack of demonstrated mechanisms of recombination, have presented technical hurdles to producing designer mtDNA mutant mouse cells [22]. To overcome these barriers, we have used a xenomitochondrial cybrid cell model which has a nuclear genome from Mus musculus and mtDNA from Rattus norvegicus ('Rn' xenocybrid). The Rn xenocybrid contains 453 amino acid changes in its 13 mtDNA-encoded subunits compared to M. musculus, resulting in nuclear/mtDNA incompatibilities that cause severe mitochondrial OXPHOS defects [23]. Although the multiple amino acid changes in xenocybrid cells do not model single pathogenic mtDNA mutations per se, they are a valuable tool for investigating OXPHOS complex deficiencies [24]. Furthermore, the xenocybrid system can be transferred to mouse ES cells to generate live xenomitochondrial mouse models for comparative in vivo studies [25].

We have used Rn xenocybrid cells here to investigate the effects of OXPHOS deficiencies on cell death and ROS generation. Rn xenocybrids have disrupted assembly of the OXPHOS complexes, with reduced steady-state levels of mature complexes I, III and IV. This is associated with complex I and III enzymatic defects and increased basal levels of ROS production. In addition, Rn xenocybrid mitochondria exhibited an increased sensitivity to C_2-ceramide compared to control cybrid mitochondria, with ceramide-mediated inhibition of OXPHOS complex III further increasing the ROS output at this complex. This inhibition could be abolished by addition of the ubiquinone analogue decylubiquinone. The ceramide-inhibition of OXPHOS function and stimulation of ROS production were associated with a four-fold higher rate of cell death compared with control cybrids cells. These results indicate that complex III defects consequent to mtDNA mutations (i.e. in the mtDNA cytochrome b gene) can increase oxidative stress and sensitivity to cell death induced by the ceramide signaling pathway.

2. Materials and methods

2.1. Reagents

Unless otherwise specified, all chemicals were purchased from Sigma (USA).

2.2. Cell lines and culture conditions

All cells were grown in RPMI 1640 medium (Life Technologies, USA) supplemented with 10% fetal bovine serum (fbs) (Life Technologies), 4.5 g/L glucose, 50 mg/L uridine and 1 mM pyruvate (RPMI/GUP medium) at 37 °C and 5% CO_2. Mouse xenocybrids were created by fusing a mtDNA-less cell line (ρ^0) with a variety of cytoplast donors. The ρ^0 clone used in these experiments, designated LMEB3, was produced from the parental line LMTK$^-$ by exposure to ethidium bromide [26]. A *Mus musculus domesticus* primary fibroblast line was used as a mitochondrial donor to create a control cybrid while a *R. norvegicus* mammary tumor line (RN1T, obtained from ATCC) was used to create a cybrid with a severe respiratory defect (Rn xenocybrid). These lines, fusions and resulting xenocybrids are described in detail elsewhere [23]. For cell death induction experiments, cells were grown in RPMI 1640 medium supplemented with 1% fbs and 2 mM L-Glutamine (treatment medium) with the addition of 25 μM C_2-ceramide (25 mM stock solution in DMSO) or 150 nM staurosporine (150 μM stock in DMSO) for the times indicated. Final concentration of DMSO in the treatment medium was 0.1% (v/v).

2.3. Radiolabeling of mitochondrial DNA-encoded subunits

Mitochondrial DNA-encoded translation products were specifically labeled as described previously [27]. In brief, cells were pretreated with 50 μg/mL chloramphenicol (CAP) in DMEM containing 10% (v/v) fbs for 24 h before incubation with 0.1 mg/mL cycloheximide in methionine-free DMEM containing 5% (v/v) dialyzed fbs for 15 min at 37 °C. Labeling was performed by the addition of 20 μCi of ^{35}S-methionine/^{35}S-cysteine (EXPRE^{35}S^{35}S Protein Labeling Mix; Perkin Elmer Life Sciences, USA) for 2 h, followed by addition of cold methionine to a final concentration of 1 mM. After 15 min, the solution was removed and replaced with DMEM/5% (v/v) fbs for extended chase times.

2.4. Blue native polyacrylamide gel electrophoresis (BN-PAGE)

BN-PAGE was performed as described with minor modifications [28]. Mitochondria (50 μg protein) were solubilized for 30 min on ice in 50 μL of 20 mM Bis–Tris pH 7.4, 50 mM NaCl, 10% (v/v) glycerol containing 1% (v/v) Triton X-100. Insoluble material was removed by centrifugation at 18000 *g* for 5 min at 4 °C, with the soluble component combined with BN-PAGE loading dye (final concentrations: 0.5% (w/v) Coomassie Blue G, 50 mM ε-amino n-caproic acid, 10 mM Bis–Tris pH 7.0) and separated on a 4–13% acrylamide–bisacrylamide BN-PAGE gel made up in 70 mM ε-amino n-caproic acid, 50 mM Bis–Tris (pH 7.0). For separation, cathode buffer (15 mM Bis–Tris pH 7.0, 50 mM tricine) containing 0.02% (w/v) Coomassie Blue G was used until the dye front had reached approximately one-third of the way through the gel before exchange with colorless cathode buffer. Anode buffer contained 50 mM Bis–Tris pH 7.0. Native complexes were separated at 100 V/5 mA for 13.5 h at 4 °C. For two-dimensional PAGE, BN-PAGE strips were positioned into the stacker of a 10–16% polyacrylamide Tris–tricine gradient gel. Samples were separated in the 2nd dimension at 100 V/25 mA for 14 h.

2.5. Western transfer and immunodetection

Western blotting was performed using a semi-dry transfer method [29] with modifications as previously described [30]. Mouse monoclonal antibodies to mitochondrial respiratory chain subunits (Life Technologies) included the α-subunit (complex V), NDUFS2 (complex I), SDHA (complex II), Core I (complex III) and CO1 (complex IV). Rabbit polyclonal antibodies to human NDUFA9 were raised against recombinant, bacterially expressed protein as previously described [31]. Secondary probing with anti-mouse or anti-rabbit HRP conjugated antibody was performed for 2 h followed by detection using ECL reagents (GE Healthcare, NJ, USA) and a MicroChemi Imaging System (DNR Bio-Imaging Systems, Israel).

2.6. Cell death markers

Hoechst 33342 staining was performed on cells grown in 8-well chamber slides. Cells were washed in ice cold PBS, treated for 5 min

in the dark at 37 °C and 5% CO_2 with 10 μg/ml Hoechst 33342 in 1× binding buffer (10 mM HEPES pH 7.4, 150 mM NaCl, 5 mM KCl, 1 mM $MgCl_2$, 1.8 mM $CaCl_2$), then washed twice for 2 min in 1× binding buffer. Cells were visualized and counted using UV excitation (340–380 nm) on a Leica DMRB microscope.

Caspase-3 activity was measured using the 'EnzChek Caspase-3 Assay Kit #1' (Life Technologies) following the manufacturer's instructions.

2.7. Isolation and electrophoresis of DNA for DNA laddering assay

DNA was isolated from cell pellets by phenol/chloroform extraction following proteinase K digestion as previously described [26]. 10 μg of DNA was resolved in a 2% agarose gel in 1× TAE at 70 V.

2.8. Mitochondrial isolation

Cell cultures were expanded to around 10^9 cells in roller bottles and mitochondria isolated using digitonin lysis and differential centrifugation [23]. Final mitochondrial preparations were resuspended to around 20 mg/mL protein in isolation buffer and frozen in aliquots at −80 °C. Preparations of sub-mitochondrial particles (SMPs) used for enzyme activity and ROS assays were created by thawing the mitochondrial preparations and diluting to 1 mg/mL in isolation buffer.

2.9. Determination of respiratory chain activities and ceramide inhibition

Determination of OXPHOS complex I, II, II + III, and III activities were as previously described [32]. For complex I, n-dodecyl β-D-maltoside was included in the reaction mixture at a concentration of 0.01% (w/v) and rotenone-sensitive activity was determined with the addition of 1 μg/ml rotenone. For ceramide inhibition experiments, C_2-ceramide was added to the reaction mixtures prior to initiating enzyme activity. In some complex II + III assays (which utilize endogenous ubiquinone as the electron carrier), the endogenous ubiquinone was supplemented by adding 0.5 to 50 μM exogenous decylubiquinone.

2.10. Fluorimetric determination of ROS production in isolated mitochondria using DCFH

2′,7′-Dichlorodihydrofluoroscein diacetate (H_2DCFDA) (Life Technologies, USA) was dissolved in DMSO at 50 mM. A 200 μM DCFH solution was created by diluting the 50 mM H_2DCFDA stock solution to 1 mM in methanol (100 μL), then adding 400 μL of 10 mM NaOH. This solution was left at room temperature for 30 min to deacetylate. The resulting 200 μM DCFH was used within 1 h for the detection of complex I- and complex III-mediated H_2O_2 generation. Complex I and III assays were performed as described above except that KCN, a known inhibitor of superoxide dismutase [33], was omitted and superoxide dismutase added at 10 U/mL. Complex I and III activities (in a reaction mixture of 950 μL) were allowed to proceed for 5 min before the addition of 50 μL of 200 μM DCFH and incubation at 30 °C for 2 h. H_2O_2-mediated oxidation of DCFH to fluorescent DCH was measured in 300 μL aliquots of the reaction mixtures using a Wallac Victor^2 1420 plate reader (excitation 485 nm/emission 535 nm). Where required, the following additions and deletions were made to the 1 mL complex I and III reaction mixtures prior to initiating the enzyme complex activities: 30 U catalase added; 25 μM C_2-ceramide (or an equal volume of DMSO) added; SMPs omitted and replaced with an equal volume of isolation buffer; 10 mM KCN added.

All complex I and III DCFH oxidation results are SMPs-dependent and catalase-sensitive.

2.11. Protein structure modeling

Amino acid differences between M. musculus and R. norvegicus in the mtDNA-encoded cytochrome b protein were modeled using the Deep View — Swiss-PDB Viewer [34].

3. Results

3.1. The Rn xenocybrid has reduced levels of steady-state OXPHOS complexes

To determine the steady-state levels of the respiratory chain complexes, isolated Mm control cybrid or Rn xenocybrid cell mitochondria were solubilized in Triton X-100 followed by blue native polyacrylamide gel electrophoresis (BN-PAGE) and Western blot analysis (Fig. 1A). In this detergent the respiratory chain complexes mainly resolve in their monomeric forms (or as a homodimer for complex III_2 [30]). The amount of mature complex I and complex IV in Rn xenocybrid mitochondria was severely decreased compared to control, with the complex III_2 dimer undetectable under these conditions. This is consistent with the complex I, II + III and IV enzymatic defects previously described in these xenocybrid cells [23].

3.2. The Rn xenocybrid has defects in OXPHOS complex biogenesis

Pulse-chase radiolabeling was performed to examine mtDNA-encoded protein translation and the subsequent assembly of these newly-translated products into their respective mature OXPHOS complexes. Labeling was conducted for 2 h, followed by a chase of either 0 or 24 h (Fig. 1B). Compared to the control Mm cybrid (Fig. 1B, lane 1), the Rn xenocybrid (lane 3) exhibited reduced amounts of newly-translated CO2, CO3 and cyt b (as has been shown previously [23]). The translation of the other mtDNA-encoded subunits of complex I (ND1, ND2, ND3, ND5, ND6), complex IV (CO1) and complex V (ATP6 and ATP8) was similar in control Mm cybrid and Rn xenocybrid mitochondria. Of note, ND4L and ATP8 resolve at the same position in Mm cybrid mitochondria (Fig. 1B, lanes 1 and 2) but at different positions in Rn xenocybrid mitochondria (lanes 3 and 4) under these electrophoresis conditions.

We next performed 2D native-PAGE analysis to examine the assembly of these newly-translated protein subunits into their respective OXPHOS complexes (Fig. 1C). In control Mm cybrid mitochondria at 0 h chase (top left panel), CO1 is found in a complex IV (CIV) assembly intermediate (CIV_i) and also mature CIV with CO2 and CO3. Cyt b is assembled quickly into the mature complex III dimer ($CIII_2$) with ATP6 and 8 assembled into mature complex V (CV). At this time point the complex I (CI) subunit ND2 is detected in a ~600 kDa assembly intermediate.

In comparison, CO1 is detected predominantly in the CIV intermediate (CIV_i) and not mature CIV in Rn xenocybrid mitochondria at 0 h chase (Fig. 1C, top right panel). Similarly, both cyt b and ND2 are also found in lower molecular weight assembly intermediates of ~440 and ~400 kDa respectively.

Following 24 h chase, CO1, 2 and 3 have fully assembled into mature CIV in Mm mitochondria, with ND1, 2, 4 and 5 detected in mature CI (Fig. 1C, bottom left panel). However, the assembly profile in Rn xenocybrid mitochondria following 24 h chase was different, with CO1 also detected not only in mature CIV but also in two CIV assembly intermediates (Fig. 1C, bottom right panel). No mature complex I (CI) is detectable, with ND2 in ~600 and ~440 kDa complex I intermediates. Furthermore, cyt b did not assemble into the complex III dimer ($CIII_2$) and was undetectable following 24 h chase.

These results suggest that the assembly of OXPHOS complexes I, III and IV is less efficient in Rn xenocybrid mitochondria, with newly-translated subunits 'stalled' in intermediate complexes. Furthermore, unassembled subunits, such as cyt b, appear to be turned-over.

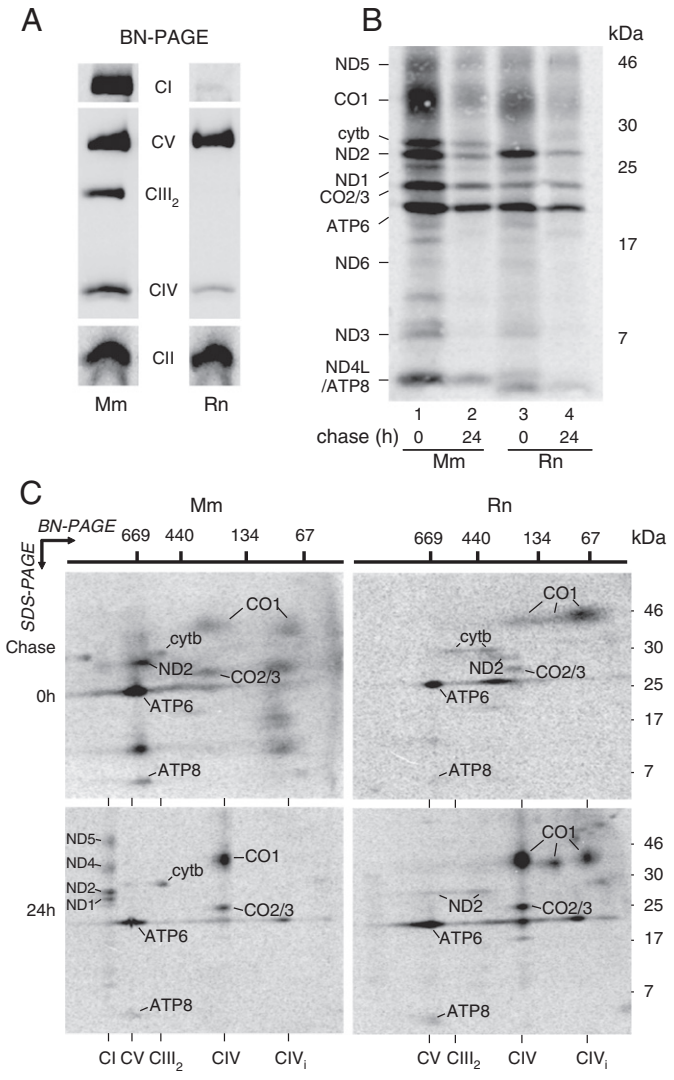

Fig. 1. OXPHOS complex assembly is disrupted in Rn xenocybrid cells. (A) Control Mm cybrid and Rn xenocybrid mitochondria were solubilized in 1% Triton X-100, followed by BN-PAGE and Western blotting. Steady-state levels of complex I (CI), the complex III dimer ($CIII_2$) and complex IV (CIV) are reduced in Rn xenocybrid mitochondria. (B) MtDNA-encoded subunits in control Mm cybrid and Rn xenocybrid cells were pulse labeled for 2 h with chase times of 0 or 24 h before separation by SDS-PAGE. Translation of CO2, CO3 and cytb is affected in Rn xenocybrids (lane 3). (C) 2D native-PAGE of pulse-chase labeled mtDNA-encoded translation products. The assembly of CO1 (complex IV), cytb (complex III) and ND2 (complex I) into their respective mature complexes appears stalled. In addition, no complex I (CI) is detectable in Rn xenocybrid mitochondria following 24 h chase (bottom right panel). CV = complex V, CIV_i = complex IV intermediate.

3.3. Ceramide-induced cell death is greatly increased in Rn xenocybrids

To determine if the OXPHOS assembly and activity defects in Rn xenocybrids have any effects on cell death induction, we treated control Mm cybrid, Rn xenocybrid and LMEB3 mtDNA-less (ρ^0) cells with the protein kinase C inhibitor staurosporine (STS, 150 nM) or C_2-ceramide (ceramide, 25 μM) for 4 h (Fig. 2A). Chromatin condensation (as a marker of cell death) was assessed by Hoechst 33342 staining [35]. Staurosporine treatment resulted in 28.7 ± 9.4% cell death in control Mm cybrids (Fig. 2A, lane 4) which exhibited classic apoptotic features, such as plasma membrane blebbing and the formation of apoptotic bodies (Supplemental Fig. 1). However, Rn xenocybrid cells were resistant to staurosporine, with only 4.1 ± 0.9% cell death in Rn xenocybrid cells (Fig. 2A, lane 5). LMEB3 ρ^0 cells were also resistant to staurosporine-induced cell death (lane 6), consistent with previous studies using human ρ^0 osteosarcoma cells [36].

Conversely, ceramide treatment induced a significant 12-fold increase in cell death in Rn xenocybrids (16.5 ± 5.2 %) (Fig. 2A, lane 8). This cell death did not exhibit any apoptotic features and was more consistent with a necrotic phenotype, including increased cell volume, enlarged nuclei and condensed chromatin (Supplemental Fig. 1). Ceramide treatment had no effect on control Mm cybrids or LMEB3 ρ^0 cells (Fig. 2A, lanes 7 and 9).

We also treated cells with staurosporine or ceramide in the presence of the media supplement B-27 (Life Technologies), which contains a cocktail of antioxidants including catalase, superoxide dismutase, DL-α tocopherol acetate, L-carnitine HCl and reduced glutathione. In the presence of these antioxidants, ceramide induced cell death of Rn xenocybrids was completely attenuated (Fig. 2B, lane 8). Staurosporine induced cell death in control Mm cybrids was also reduced in the presence of B-27, albeit incompletely (12.1 ± 3.6% death, Fig. 2B, lane 4).

To determine the type of cell death induced by ceramide we investigated whether chromosomal DNA fragmentation (a hallmark of apoptosis) was occurring in Rn xenocybrid cells (Fig. 2C). No DNA fragmentation was observed after 24 h ceramide treatment in control Mm cybrids (Fig. 2C, lane 8), Rn xenocybrids (lane 9) or LMEB3 ρ^0 cells (lane 10). In comparison, DNA laddering is clearly evident in control Mm cybrids following 16 h staurosporine treatment (Fig. 2C, lane 5).

We next determined whether ceramide induced apoptotic cell death by examining plasma membrane phosphatidylserine exposure (Fig. 2D). Control Mm cybrid cells exhibited only background annexin-FITC staining after either 2.5 h (Fig. 2D, lane 3) or 4.5 h (lane 5) ceramide treatment. Propidium iodide staining detected only 5.6% dead control Mm cybrid cells after 4.5 h ceramide treatment (data not shown), consistent with our experimental findings using Hoechst staining (Fig. 2A). Rn xenocybrid cells exhibited minimal positive annexin-FITC staining after only 2.5 h ceramide treatment (2.4 ±0.2%, lane 4) which returned to background levels after 4.5 h treatment (0.4 ± 0.2%, lane 6). In comparison, 4 h of staurosporine treatment in control Mm cybrids induced phosphatidylserine exposure in 16.9 ±2.7% of cells (Fig. 2D, lane 7) but only 2.6 ± 0.3% in Rn xenocybrids (lane 8).

We also examined whether the apoptotic protease cascade, in the form of caspase-3 activity, was induced in Rn xenocybrids by ceramide (Fig. 2E). Treatment of either control Mm cybrid or Rn xenocybrid cells with ceramide for 6 h did not increase caspase-3 activity compared to untreated cells (Fig. 2E, lanes 3 and 4). This suggests that ceramide induced cell death is independent of the caspase cascade in these cells, as treatment of control Mm cybrids with staurosporine for 3 h resulted in a 10-fold induction of caspase-3 activity (Fig. 2E, lane 5).

Taken together, these results suggest that ceramide induced cell death in Rn xenocybrid cells is not apoptotic but is more consistent with a necrotic phenotype.

3.4. Inhibition of OXPHOS complex III by ceramide in Rn xenocybrid mitochondria

To determine if ceramide induction of cell death in Rn xenocybrids was due to direct inhibition of OXPHOS activity, we performed enzymatic assays in the presence of 25 μM C_2-ceramide (Fig. 3). Complex I activity was ~30% slower in Rn xenocybrid mitochondria compared to control Mm mitochondria (as discussed previously [23]) however this was not significantly different ($p = 0.28$) (Fig. 3A, lanes 1 and 2). Furthermore, this activity was not affected by the presence of ceramide in either Mm or Rn mitochondria (Fig. 3A, lanes 3 and 4).

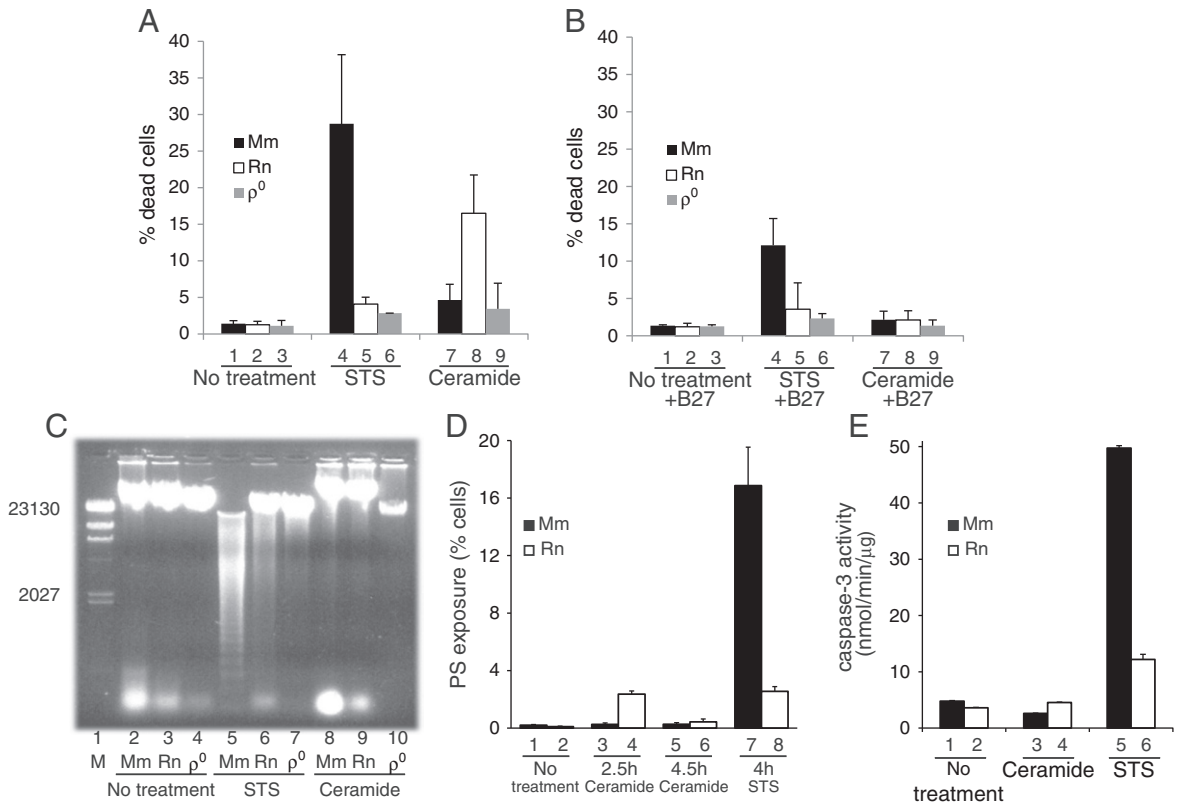

Fig. 2. Ceramide induces cell death in Rn xenocybrid cells. (A) Control Mm cybrid (■), Rn xenocybrid (□) and LMEB3 ρ^0 (■) cells were incubated with either 150 nM staurosporine (STS) or 25 μM C_2 ceramide for 4 h, followed by Hoechst 33342 staining. Rn xenocybrid cells show greatly increased cell death from ceramide, while only control Mm cells are sensitive to STS. (B) Control Mm cybrid (■), Rn xenocybrid (□) and LMEB3 ρ^0 (■) cells were incubated with either 150 nM STS or 25 μM C_2 ceramide in the presence of the media supplement B-27 for 4 h, followed by Hoechst 33342 staining. Ceramide-induced cell death of Rn xenocybrid cells was completely abolished by the B-27 antioxidants. (C) Control Mm cybrid, Rn xenocybrid and LMEB3 ρ^0 cells were treated with 150 nM STS for 16 h or 250 μM C_2 ceramide for 24 h. Total DNA was extracted with 10 μg loaded per lane. Chromosomal DNA fragmentation was only observed in control Mm cybrids after treatment with STS (lane 5). M = DNA marker. (D) Control Mm cybrid (■) and Rn xenocybrid (□) cells were treated with 25 μM C_2 ceramide or 150 nM STS for the times indicated, then stained with annexin-FITC/propidium iodide. Plasma membrane phosphatidylserine (PS) exposure was not induced by ceramide, and was only evident following STS treatment of control Mm cybrids (lane 7). (E) Control Mm cybrid (■) and Rn xenocybrid (□) cells were treated with 25 μM C_2 ceramide for 6 h or 150 nM STS for 3 h. Caspase-3 activity was not induced in control Mm cybrids or Rn xenocybrids by ceramide. Conversely, caspase-3 activity is induced in control Mm cybrids in response to STS (lane 5). All histogram data is expressed as mean ± s.d. (n = 3).

Complex II activities of both Mm and Rn mitochondria were also not affected by ceramide (Fig. 3B, lanes 3 and 4).

Complex II + III activity was 39% slower in untreated Rn xenocybrid mitochondria compared to untreated control Mm mitochondria ($p < 0.05$) (Fig. 3C, lanes 1 and 2), with a similar deficiency measured by the complex III assay ($p < 0.05$) (Fig. 3D, lanes 1 and 2). Of note, complex II + III activity was almost totally inhibited by ceramide (3% residual activity) in Rn xenocybrid mitochondria, compared to control Mm mitochondria which were unaffected (Fig. 3C, lanes 3 and 4). Complex III activity was also reduced in Rn xenocybrid mitochondria by ceramide, albeit not significantly (Fig. 3D, lanes 3 and 4).

The level of ceramide-mediated inhibition of complex II + III activity in Rn xenocybrid mitochondria was concentration-dependent, with an apparent IC_{50} of ~6.2 μM (Fig. 4A). Control Mm cybrid mitochondria showed a slight sensitivity to ceramide at the highest concentration used (~25% inhibition at 50 μM) but this was not statistically significant ($p = 0.13$).

The substantial ceramide-mediated inhibition of Rn xenocybrid II + III activity (85% inhibition with 10 μM ceramide) was abolished by including 10 μM exogenous decylubiquinone (DB) in the II + III assay (Fig. 4B). Of note, the inclusion of up to 50 μM DB alone (in the *absence* of ceramide) had no effect on complex II + III activity in Mm control or Rn xenocybrid mitochondria (data not shown).

These results show that ceramide can directly inhibit complex III activity in Rn xenocybrid mitochondria due to species-specific differences in complex III composition and structure. In addition, this inhibition can be rescued by decylubiquinone, suggesting that ceramide binding to the ubiquinone site of complex III is enhanced in the xenocybrid compared with wild-type complex III.

3.5. Reactive oxygen species production by complex III is elevated in Rn xenocybrid mitochondria and further stimulated by ceramide

We next assessed whether ceramide treatment can induce reactive oxygen species generation in Rn xenocybrid mitochondria during the stimulation of either complex I or complex III activity. Complex I-mediated DCFH oxidation appeared slightly higher in Rn xenocybrid mitochondria compared to control Mm mitochondria (Fig. 5A, lanes 1 and 2). However, as per the complex I activity data (Fig. 3A), this was not a statistically significant difference ($p = 0.72$). Additionally, the presence of ceramide had no effect on complex I-mediated DCFH oxidation in either control Mm or Rn mitochondria (Fig. 5A, lanes 3 and 4).

In the absence of ceramide, the rate of complex III-mediated DCFH oxidation was 66% higher in Rn xenocybrid mitochondria compared to control Mm cybrid mitochondria ($p < 0.05$) (Fig. 5B, lanes 1 and 2). However, the addition of ceramide increased this rate further by 42% in Rn xenocybrid mitochondria ($p < 0.01$) (Fig. 5B, lane 4). Conversely, the presence of ceramide had no effect on DCFH oxidation by control Mm cybrid mitochondria ($p = 0.36$) (Fig. 5B, lane 3). DCFH oxidation was abolished when 10 mM KCN, an inhibitor of superoxide dismutase [33], was included in the complex III assay

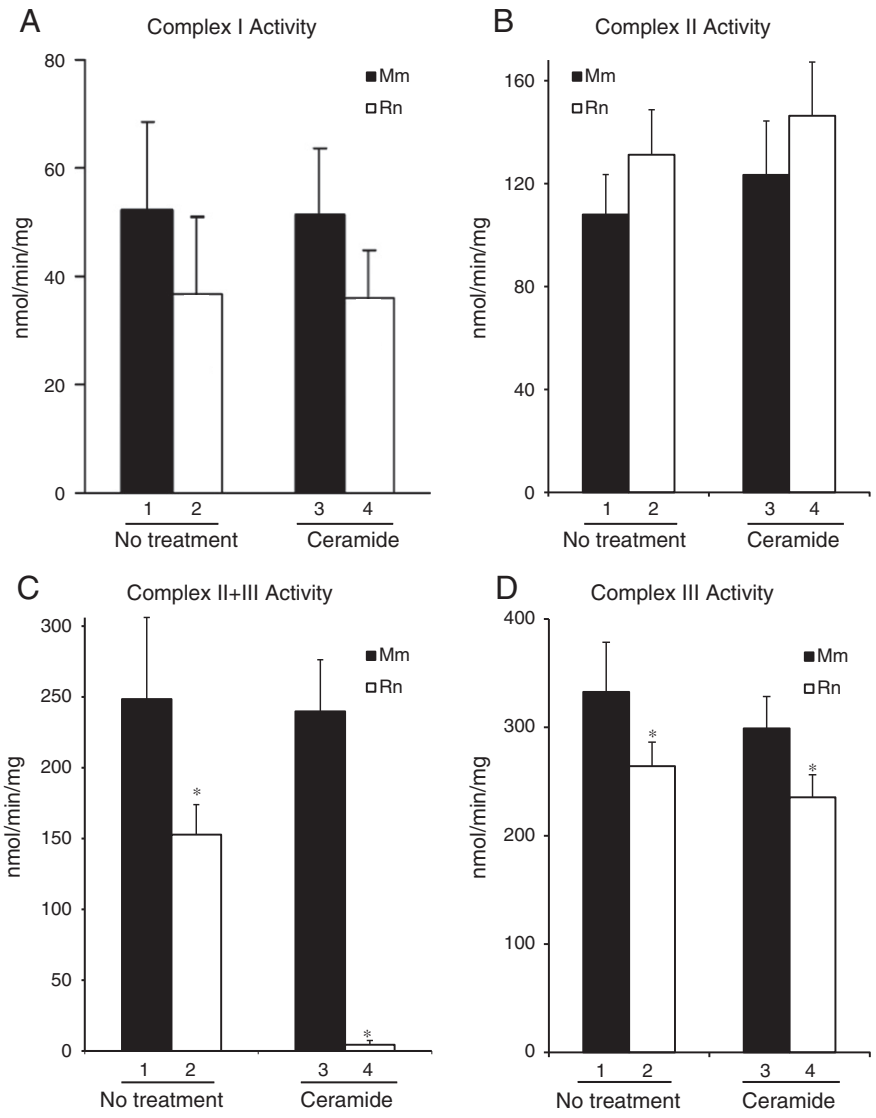

Fig. 3. Inhibition of complex III activity by ceramide in Rn xenocybrid cells. Complex I (A), complex II (B), complex II + III (C) and complex III (D) activities of control Mm cybrid (■) and Rn xenocybrid (□) mitochondria were measured spectrophotometrically in the presence or absence of 25 μM C_2 ceramide. Complex II + III and III activities were significantly lower in untreated Rn xenocybrid mitochondria compared to control Mm cybrid mitochondria, with complex II + III activity in Rn xenocybrid mitochondria almost completely inhibited by ceramide (C, lane 4). Data is expressed as mean ± s.d. (n = 5). *$p < 0.05$.

(Fig. 5B, lanes 5 and 6), suggesting the ultimate oxidation of DCFH is due to an initial output of superoxide.

These results indicate that the species-specific differences in Rn xenocybrid mitochondria result in increased superoxide generation at complex III which is further elevated in the presence of ceramide.

4. Discussion

Mitochondria play an integral role in cell death signaling of both apoptotic and necrotic pathways. The intrinsic apoptotic pathway (also known as the BLC-2 or mitochondrial pathway) is activated by developmental cues or cytotoxic insults (*e.g.* increased intracellular Ca^{2+} or ROS) which activates pro-apoptotic BCL-2 family members such as BAX and BAK. In a process which is not yet fully understood, BAX and BAK induce mitochondrial outer membrane permeabilization (MOMP), resulting in the release of pro-apoptotic molecules such as SMAC/DIABLO and cytochrome *c* into the cytosol [37]. Cytochrome *c* then induces the formation of the apoptosome and the activation of caspase-9 [38].

Alternatively, the extrinsic or death receptor pathway (induced by Fas or TNF receptor ligation) can also promote cell death *via* mitochondrial signaling. These receptors can recruit and activate the Fas-associated death domain (FADD) which in turn can activate caspase-8. Caspase-8 can then cleave BID to form its C-terminal truncated form (tBID) which translocates to the mitochondria to induce MOMP and downstream caspase activation [38].

Studies using mtDNA-less ρ^0 cells have highlighted the importance of mitochondrial function in apoptotic signaling and execution. The total lack of OXPHOS in these cells is usually found to increase resistance to apoptosis induced by various agents [16,36,39–42]. Nevertheless, Wang et al. also showed that human osteosarcoma ρ^0 cells can be as sensitive as parental ρ^+ cells to TNFα or Fas ligation if co-treated with actinomycin D [43].

However, these models do not address the question of whether OXPHOS defects can produce pathologic effects by increasing mitochondrial ROS, or by other effects consequent to altered binding of signaling molecules to the OXPHOS proteins which are largely absent in the mtDNA depletion models. Most mitochondrial diseases result from point mutations affecting single gene products, and deletions or tRNA mutations affecting all gene products (for reviews see [44,45]). Our results suggest that the pathophysiology of mitochondrial diseases could in part result from very different effects on cell

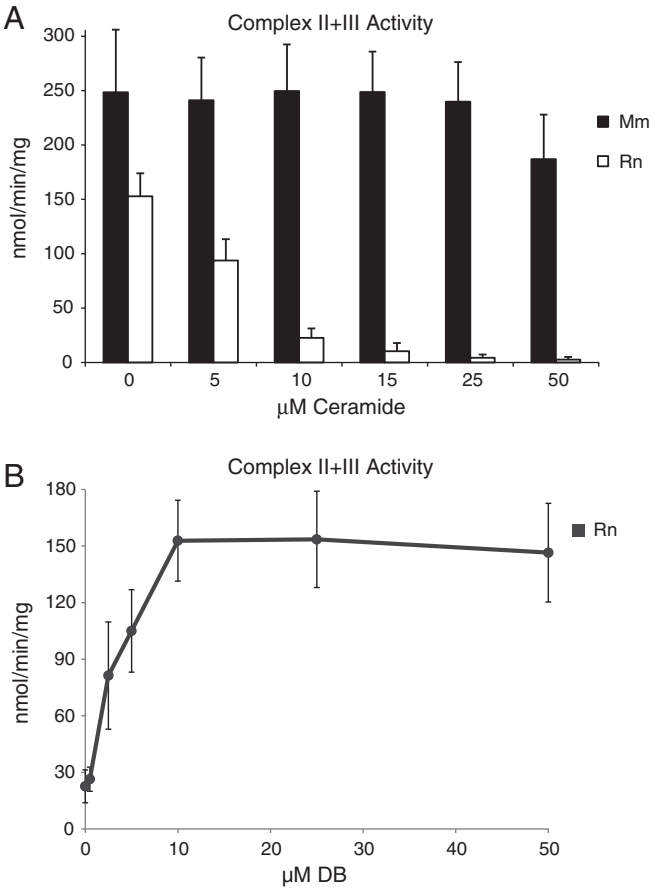

Fig. 4. Inhibition of complex II + III activity in Rn xenocybrid mitochondria by ceramide can be offset with decylubiquinone. (A) Control Mm cybrid (■) and Rn xenocybrid (□) mitochondria were treated with increasing concentrations of C_2 ceramide as indicated. 10 μM C_2 ceramide inhibits complex II + III activity in Rn xenocybrid mitochondria by 85%. Activity in control Mm cybrid mitochondria is not affected, even by 50 μM ceramide ($p = 0.13$). (B) Rn xenocybrid mitochondria were treated concurrently with 10 μM C_2 ceramide and increasing concentrations of decylubiquinone (DB) as indicated. 10 μM DB was sufficient to attenuate the ceramide inhibition of complex II + III activity in Rn xenocybrid mitochondria. Data is expressed as mean ± s.d. ($n = 4$).

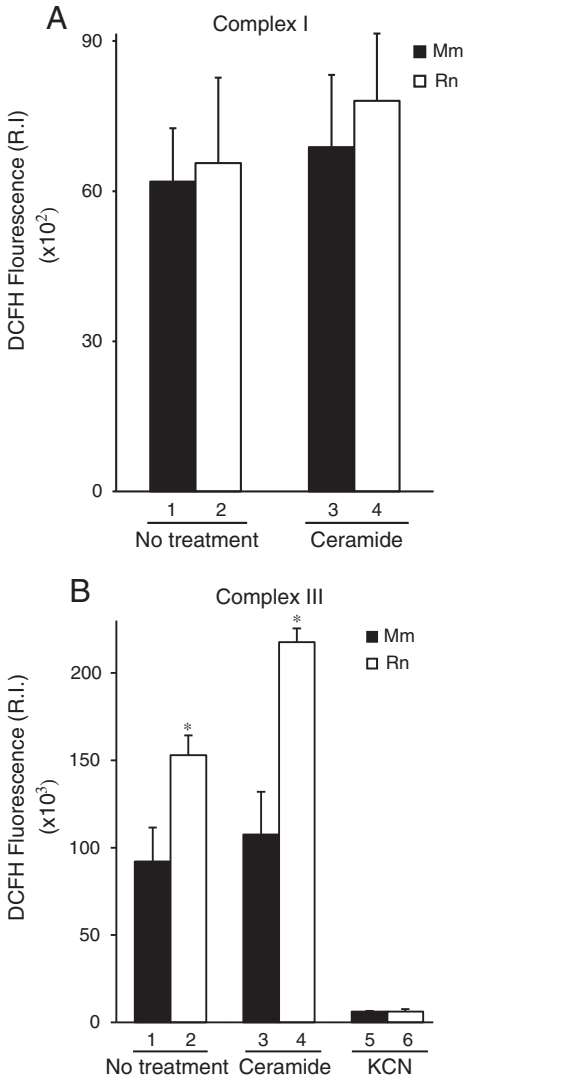

Fig. 5. Reactive oxygen species production is elevated in Rn xenocybrids and further stimulated by ceramide. (A) Complex I and (B) III assays were performed with control Mm cybrid (■) and Rn xenocybrid (□) mitochondria in the presence or absence of 25 μM C_2 ceramide. H_2O_2 production was measured by following the rate of oxidation of DCFH at 485/520 nm. H_2O_2 production was not significantly different in Rn xenocybrid mitochondria compared to control Mm cybrid mitochondria when complex I activity was stimulated in either the presence or absence of ceramide (A). (B) The rate of H_2O_2 generation was 66% higher in Rn xenocybrid mitochondria compared to control Mm mitochondria when complex III activity was stimulated (lane 2). This rate was further increased by 42% in the presence of ceramide (lane 4). Addition of the superoxide dismutase inhibitor KCN abolished the oxidation of DCFH (lanes 5 and 6). Data is expressed as mean ± s.d. ($n = 4$). *$p < 0.05$.

death signaling to those found in mtDNA depletion models. We show here direct evidence for an enhanced cytotoxic effect of ceramide consequent to an altered mtDNA-encoded protein; the apocytochrome *b* of complex III.

For these studies we have used our Rn xenocybrid model, where mismatches between the mouse nuclear-encoded OXPHOS subunits and the rat mtDNA-encoded subunits results in multiple OXPHOS defects [23]. Although this model does not directly mimic single pathogenic mtDNA mutations, it enables modeling of mtDNA-derived OXPHOS defects in mouse cells in the face of limitations in current technology for mtDNA manipulation [22].

Interestingly, although relatively mild enzymatic deficiencies of complex I (~70% residual activity) and complex III (~79%) were measured in Rn xenocybrid mitochondria, the steady-state levels of both complexes were virtually undetectable by BN-PAGE (Fig. 1A). This discrepancy may be due to the altered stability of these xeno-complexes. The multiple amino acid changes in their mtDNA-encoded protein subunits will destabilize their structures, however the mature complexes are still relatively intact and active *in vivo*. On the other hand, this destabilization results in the complexes falling apart under the BN-PAGE conditions used, and as such they are not detected in their mature forms. We have observed this phenomenon previously, whereby mitochondrial membrane lipid changes result in the destabilization of the OXPHOS supercomplex, resulting in the loss of the mature supercomplex under certain BN-PAGE conditions [46].

The OXPHOS defects in the Rn xenocybrid cells resulted in reduced sensitivity to staurosporine-induced cell death with no activation of caspase-3. This cell death was similar to mouse LMEB3 ρ^0 cells, in agreement with previous reports using human ρ^0 cells [36]. These findings suggest that staurosporine-induced apoptosis is partly dependent on OXPHOS function. Conversely, the defective OXPHOS function in the Rn xenocybrids switched them to a ceramide sensitive phenotype (with both the control Mm cybrid and ρ^0 cells resistant to ceramide-induced cell death).

The Rn xenocybrid OXPHOS defects were also associated with an increase in basal H_2O_2 production. In addition, treatment with ceramide further inhibited OXPHOS function and increased ROS production. Most striking was our finding that the presence of the

mismatched *Rattus* cytochrome *b* gene product increased complex III inhibition by ceramide, with almost complete abolition of electron transfer within the complex.

Some controversy exists around observations of ceramide interactions with OXPHOS complexes. Direct assays [20] and indirect approaches using specific respiratory chain complex inhibitors [15,16,19] have implicated complex III as a site of ceramide inhibition. Other studies have implicated complex I inhibition and have questioned the findings of Gudz et al. [20] regarding complex III inhibition [21]. It has been noted that ceramide analogs may interact with cytochrome *c in vitro*, decreasing the apparent reducibility of the electron carrier [21,47], but this interaction was not evident when cytochrome *c* was added in our assays.

Our data suggests that ceramide interaction with complex III is altered by one or more of the 26 amino acid differences between the mouse and rat apocytochrome *b* gene products (Supplementary Table 1), greatly increasing the inhibition of enzymatic activity while stimulating ROS production by the complex. Interestingly, this inhibition could be completely attenuated by addition of the ubiquinone analogue decylubiquinone, suggesting that ceramide competes with ubiquinone for complex III binding and that the *Rattus* amino acid substitutions in cytochrome *b* alter this interaction.

We have modeled the *Rattus* amino acid changes in cytochrome *b* (shown in green) using the structure of bovine complex III with bound ubiquinone as a template (Supplemental Fig. 2). Although none of the *Rattus* amino acid substitutions (red) are of residues that interact with ubiquinone within its binding sites Q_i and Q_o, they are found in a region adjacent to the Q_i site that is important for the interaction of cytochrome *b* with cytochrome c1 (shown in dark blue, Supp. Fig. 2A). These substitutions are likely to both destabilize holocomplex III and make the Q_i site more accessible to ceramide. In particular, *Rattus* amino acid substitutions at positions 229 (Leu) and 232 (Val) are found directly adjacent to the Qi site (Supplemental Fig. 2B).

Ceramide is commonly regarded as a second messenger in some apoptotic pathways, with sphingolipid metabolism recently identified as essential for the activation of BAX/BAK-dependent cytochrome *c* release [48]. Ceramide-induced cell death can be either caspase-dependent or independent [49,50] and may or may not result in internucleosomal DNA cleavage [13,51]. In our Rn xenocybrid model ceramide-induced cell death lacked the apoptotic signatures of caspase-3 activation and chromosomal DNA cleavage and was more consistent with regulated necrosis or 'necroptosis' [52]. Unlike apoptosis (which requires ATP), this form of cell death can be initiated under ATP-depleted conditions [53], as found in our Rn xenocybrid cells.

We also found that ceramide-induced death of Rn xenocybrid cells could be completely attenuated by antioxidants, suggesting that the ROS generated is critical for cell death induction. Without scavenging, this ceramide-induced ROS can lead to cellular damage, including lipid peroxidation of cellular membranes [54]. The formation of these lipid hydroperoxides can induce lysosome membrane permeabilization, resulting in the leakage of cytotoxic hydrolases into the cytosol and the induction of cell death [52]. Lipid peroxidation products can also induce mitochondrial inner membrane permeabilization, resulting in the dissipation of $\Delta\psi_m$ and reduced Ca^{2+} buffering capacity [55]. This leakage of proteases and Ca^{2+} into the cytosol are two important factors that contribute to necroptotic cell death.

We speculate that the OXPHOS-derived increase in ROS, due to ceramide inhibition of complex III activity, is the trigger for increased necroptotic cell death in Rn xenocybrids. Mitochondrial ATP production is significantly diminished in these cells, yet clearly not more than in the mouse ρ^0 cells (which have no mitochondrial ATP production), suggesting reduced ATP production rate is not the primary cause of ceramide sensitivity in the Rn xenocybrids, although it may determine the *type* of cell death in this case. This is supported by previous findings using rotenone-inhibition of complex I in human osteosarcoma cells, where cell death was associated with the increased ROS production more closely than with the decreased ATP production [56].

5. Conclusions

Few reports have addressed the question of whether defective OXPHOS activity, consequent to human disease-causing mtDNA mutations, may modulate cell death pathways. One study used cybrids containing mtDNA complex I gene mutations linked to Leber Hereditary Optic Neuropathy to show a modest increase in sensitivity to cell death induced by anti-Fas antibodies [7]. Another report found greatly increased apoptosis and induction of mitochondrial SOD activity in fibroblasts from patients with the T8993A mutation in the ATP6 gene (complex V) associated with Leigh's disease/NARP [57]. Our data supports these observations and suggests one possible mechanism. In cells with OXPHOS defects, especially complex III defects, mitochondrial ceramide may more readily induce cell death, possibly consequent to increased respiratory chain-derived ROS due to competition with ubiquinone at the binding site of complex III.

Further work is needed to clarify the specificity of ceramide interaction with OXPHOS complexes, in particular complex III, and reasons for differences observed in ceramide effects between different cell types, tissues and species.

Supplementary data to this article can be found online at http://dx.doi.org/10.1016/j.bbabio.2013.03.012.

Acknowledgements

This work was supported by the Victorian Government's Operational Infrastructure Support Program, Monash Institute of Medical Research Start-up Funding (MMcK) and National Health and Medical Research Council Australia grants to IAT (Project Grant 145719) and MMcK (CDA Fellowship 541911). We thank Dick Cotton, Andrew Wilks and Mark Cook for support.

References

[1] D. Skladal, J. Halliday, D.R. Thorburn, Minimum birth prevalence of mitochondrial respiratory chain disorders in children, Brain 126 (2003) 1905–1912.
[2] J. Smeitink, L. van den Heuvel, S. DiMauro, The genetics and pathology of oxidative phosphorylation, Nat. Rev. Genet. 2 (2001) 342–352.
[3] M.D. Brown, I.A. Trounce, A.S. Jun, J.C. Allen, D.C. Wallace, Functional analysis of lymphoblast and cybrid mitochondria containing the 3460, 11778, or 14484 Leber's hereditary optic neuropathy mitochondrial DNA mutation, J. Biol. Chem. 275 (2000) 39831–39836.
[4] A.S. Jun, I.A. Trounce, M.D. Brown, J.M. Shoffner, D.C. Wallace, Use of transmitochondrial cybrids to assign a complex I defect to the mitochondrial DNA-encoded NADH dehydrogenase subunit 6 gene mutation at nucleotide pair 14459 that causes Leber hereditary optic neuropathy and dystonia, Mol. Cell. Biol. 16 (1996) 771–777.
[5] M. Degli Esposti, V. Carelli, A. Ghelli, M. Ratta, M. Crimi, S. Sangiorgi, P. Montagna, G. Lenaz, E. Lugaresi, P. Cortelli, Functional alterations of the mitochondrially encoded ND4 subunit associated with Leber's hereditary optic neuropathy, FEBS Lett. 352 (1994) 375–379.
[6] A. Wong, L. Cavelier, H.E. Collins-Schramm, M.F. Seldin, M. McGrogan, M.L. Savontaus, G.A. Cortopassi, Differentiation-specific effects of LHON mutations introduced into neuronal NT2 cells, Hum. Mol. Genet. 11 (2002) 431–438.
[7] S.R. Danielson, A. Wong, V. Carelli, A. Martinuzzi, A.H. Schapira, G.A. Cortopassi, Cells bearing mutations causing Leber's hereditary optic neuropathy are sensitized to Fas-induced apoptosis, J. Biol. Chem. 277 (2002) 5810–5815.
[8] M. Rana, I. de Coo, F. Diaz, H. Smeets, C.T. Moraes, An out-of-frame cytochrome b gene deletion from a patient with parkinsonism is associated with impaired complex III assembly and an increase in free radical production, Ann. Neurol. 48 (2000) 774–781.
[9] A. Trifunovic, A. Wredenberg, M. Falkenberg, J.N. Spelbrink, A.T. Rovio, C.E. Bruder, Y.M. Bohlooly, S. Gidlof, A. Oldfors, R. Wibom, J. Tornell, H.T. Jacobs, N.G. Larsson, Premature ageing in mice expressing defective mitochondrial DNA polymerase, Nature 429 (2004) 417–423.
[10] S. Mathias, L.A. Pena, R.N. Kolesnick, Signal transduction of stress *via* ceramide, Biochem. J. 335 (1998) 465–480.
[11] M. Iwata, J. Herrington, R.A. Zager, Sphingosine: a mediator of acute renal tubular injury and subsequent cytoresistance, Proc. Natl. Acad. Sci. U. S. A. 92 (1995) 8970–8974.

[12] A.S. Arora, B.J. Jones, T.C. Patel, S.F. Bronk, G.J. Gores, Ceramide induces hepatocyte cell death through disruption of mitochondrial function in the rat, Hepatology 25 (1997) 958–963.
[13] H. Zhou, S.A. Summers, M.J. Birnbaum, R.N. Pittman, Inhibition of Akt kinase by cell-permeable ceramide and its implications for ceramide-induced apoptosis, J. Biol. Chem. 273 (1998) 16568–16575.
[14] O. Cuvillier, L. Edsall, S. Spiegel, Involvement of sphingosine in mitochondria-dependent Fas-induced apoptosis of type II Jurkat T cells, J. Biol. Chem. 275 (2000) 15691–15700.
[15] A. Quillet-Mary, J.P. Jaffrezou, V. Mansat, C. Bordier, J. Naval, G. Laurent, Implication of mitochondrial hydrogen peroxide generation in ceramide-induced apoptosis, J. Biol. Chem. 272 (1997) 21388–21395.
[16] A. Guidarelli, E. Clementi, C. De Nadai, R. Bersacchi, O. Cantoni, TNFalpha enhances the DNA single-strand breakage induced by the short-chain lipid hydroperoxide analogue tert-butylhydroperoxide *via* ceramide-dependent inhibition of complex III followed by enforced superoxide and hydrogen peroxide formation, Exp. Cell Res. 270 (2001) 56–65.
[17] S. Corda, C. Laplace, E. Vicaut, J. Duranteau, Rapid reactive oxygen species production by mitochondria in endothelial cells exposed to tumor necrosis factor-alpha is mediated by ceramide, Am. J. Respir. Cell Mol. Biol. 24 (2001) 762–768.
[18] D.C. Phillips, K. Allen, H.R. Griffiths, Synthetic ceramides induce growth arrest or apoptosis by altering cellular redox status, Arch. Biochem. Biophys. 407 (2002) 15–24.
[19] C. Garcia-Ruiz, A. Colell, M. Mari, A. Morales, J.C. Fernandez-Checa, Direct effect of ceramide on the mitochondrial electron transport chain leads to generation of reactive oxygen species. Role of mitochondrial glutathione, J. Biol. Chem. 272 (1997) 11369–11377.
[20] T.I. Gudz, K.Y. Tserng, C.L. Hoppel, Direct inhibition of mitochondrial respiratory chain complex III by cell-permeable ceramide, J. Biol. Chem. 272 (1997) 24154–24158.
[21] M. Di Paola, T. Cocco, M. Lorusso, Ceramide interaction with the respiratory chain of heart mitochondria, Biochemistry 39 (2000) 6660–6668.
[22] R.N. Lightowlers, Mitochondrial transformation: time for concerted action, EMBO Rep. 12 (2011) 480–481.
[23] M. McKenzie, I. Trounce, Expression of *Rattus norvegicus* mtDNA in *Mus musculus* cells results in multiple respiratory chain defects, J. Biol. Chem. 275 (2000) 31514–31519.
[24] M. McKenzie, M. Chiotis, C.A. Pinkert, I.A. Trounce, Functional respiratory chain analyses in murid xenomitochondrial cybrids expose coevolutionary constraints of cytochrome b and nuclear subunits of complex III, Mol. Biol. Evol. 20 (2003) 1117–1124.
[25] M. McKenzie, I.A. Trounce, C.A. Cassar, C.A. Pinkert, Production of homoplasmic xenomitochondrial mice, Proc. Natl. Acad. Sci. U. S. A. 101 (2004) 1685–1690.
[26] I. Trounce, J. Schmiedel, H.C. Yen, S. Hosseini, M.D. Brown, J.J. Olson, D.C. Wallace, Cloning of neuronal mtDNA variants in cultured cells by synaptosome fusion with mtDNA-less cells, Nucleic Acids Res. 28 (2000) 2164–2170.
[27] M. McKenzie, M. Lazarou, M.T. Ryan, Chapter 18 analysis of respiratory chain complex assembly with radiolabeled nuclear- and mitochondrial-encoded subunits, Methods Enzymol. 456 (2009) 321–339.
[28] H. Schagger, G. von Jagow, Blue native electrophoresis for isolation of membrane protein complexes in enzymatically active form, Anal. Biochem. 199 (1991) 223–231.
[29] E. Harlow, D. Lane, Using Antibodies: A Laboratory Manual, Cold Spring Harbor Laboratory Press, Cold Spring Harbor, 1999.
[30] M. McKenzie, M. Lazarou, D.R. Thorburn, M.T. Ryan, Analysis of mitochondrial subunit assembly into respiratory chain complexes using blue native polyacrylamide gel electrophoresis, Anal. Biochem. 364 (2007) 128–137.
[31] A.J. Johnston, J. Hoogenraad, D.A. Dougan, K.N. Truscott, M. Yano, M. Mori, N.J. Hoogenraad, M.T. Ryan, Insertion and assembly of human tom7 into the preprotein translocase complex of the outer mitochondrial membrane, J. Biol. Chem. 277 (2002) 42197–42204.
[32] I.A. Trounce, Y.L. Kim, A.S. Jun, D.C. Wallace, Assessment of mitochondrial oxidative phosphorylation in patient muscle biopsies, lymphoblasts, and transmitochondrial cell lines, Methods Enzymol. 264 (1996) 484–509.
[33] M.D. Holdom, R.J. Hay, A.J. Hamilton, The Cu, Zn superoxide dismutases of *Aspergillus flavus*, *Aspergillus niger*, *Aspergillus nidulans*, and *Aspergillus terreus*: purification and biochemical comparison with the *Aspergillus fumigatus* Cu, Zn superoxide dismutase, Infect. Immun. 64 (1996) 3326–3332.
[34] N. Guex, M.C. Peitsch, SWISS-MODEL and the Swiss-PdbViewer: an environment for comparative protein modeling, Electrophoresis 18 (1997) 2714–2723.
[35] F. Belloc, P. Dumain, M.R. Boisseau, C. Jalloustre, J. Reiffers, P. Bernard, F. Lacombe, A flow cytometric method using Hoechst 33342 and propidium iodide for simultaneous cell cycle analysis and apoptosis determination in unfixed cells, Cytometry 17 (1994) 59–65.
[36] R. Dey, C.T. Moraes, Lack of oxidative phosphorylation and low mitochondrial membrane potential decrease susceptibility to apoptosis and do not modulate the protective effect of Bcl-x(L) in osteosarcoma cells, J. Biol. Chem. 275 (2000) 7087–7094.
[37] S.W. Tait, D.R. Green, Mitochondria and cell signalling, J. Cell Sci. 125 (2012) 807–815.
[38] R.J. Youle, A. Strasser, The BCL-2 protein family: opposing activities that mediate cell death, Nat. Rev. Mol. Cell Biol. 9 (2008) 47–59.
[39] M.D. Jacobson, J.F. Burne, M.P. King, T. Miyashita, J.C. Reed, M.C. Raff, Bcl-2 blocks apoptosis in cells lacking mitochondrial DNA, Nature 361 (1993) 365–369.
[40] S. Jiang, J. Cai, D.C. Wallace, D.P. Jones, Cytochrome c-mediated apoptosis in cells lacking mitochondrial DNA. Signaling pathway involving release and caspase 3 activation is conserved, J. Biol. Chem. 274 (1999) 29905–29911.
[41] M. Higuchi, B.B. Aggarwal, E.T. Yeh, Activation of CPP32-like protease in tumor necrosis factor-induced apoptosis is dependent on mitochondrial function, J. Clin. Invest. 99 (1997) 1751–1758.
[42] N. Hail Jr., R. Lotan, Mitochondrial respiration is uniquely associated with the prooxidant and apoptotic effects of N-(4-hydroxyphenyl)retinamide, J. Biol. Chem. 276 (2001) 45614–45621.
[43] J. Wang, J.P. Silva, C.M. Gustafsson, P. Rustin, N.G. Larsson, Increased *in vivo* apoptosis in cells lacking mitochondrial DNA gene expression, Proc. Natl. Acad. Sci. U. S. A. 98 (2001) 4038–4043.
[44] D.C. Wallace, Mitochondrial diseases in man and mouse, Science 283 (1999) 1482–1488.
[45] S. DiMauro, E.A. Schon, Mitochondrial DNA mutations in human disease, Am. J. Med. Genet. 106 (2001) 18–26.
[46] M. McKenzie, M. Lazarou, D.R. Thorburn, M.T. Ryan, Mitochondrial respiratory chain supercomplexes are destabilized in Barth Syndrome patients, J. Mol. Biol. 361 (2006) 462–469.
[47] P. Ghafourifar, S.D. Klein, O. Schucht, U. Schenk, M. Pruschy, S. Rocha, C. Richter, Ceramide induces cytochrome c release from isolated mitochondria. Importance of mitochondrial redox state, J. Biol. Chem. 274 (1999) 6080–6084.
[48] J.E. Chipuk, G.P. McStay, A. Bharti, T. Kuwana, C.J. Clarke, L.J. Siskind, L.M. Obeid, D.R. Green, Sphingolipid metabolism cooperates with BAK and BAX to promote the mitochondrial pathway of apoptosis, Cell 148 (2012) 988–1000.
[49] C.A. da Costa, K. Ancolio, F. Checler, Wild-type but not Parkinson's disease-related ala-53–>Thr mutant alpha-synuclein protects neuronal cells from apoptotic stimuli, J. Biol. Chem. 275 (2000) 24065–24069.
[50] N. Engedal, F. Saatcioglu, Ceramide-induced cell death in the prostate cancer cell line LNCaP has both necrotic and apoptotic features, Prostate 46 (2001) 289–297.
[51] V. Lakics, S.N. Vogel, Lipopolysaccharide and ceramide use divergent signaling pathways to induce cell death in murine macrophages, J. Immunol. 161 (1998) 2490–2500.
[52] P. Vandenabeele, L. Galluzzi, T. Vanden Berghe, G. Kroemer, Molecular mechanisms of necroptosis: an ordered cellular explosion, Nat. Rev. Mol. Cell Biol. 11 (2010) 700–714.
[53] M. Leist, B. Single, A.F. Castoldi, S. Kuhnle, P. Nicotera, Intracellular adenosine triphosphate (ATP) concentration: a switch in the decision between apoptosis and necrosis, J. Exp. Med. 185 (1997) 1481–1486.
[54] H. Zigdon, A. Kogot-Levin, J.W. Park, R. Goldschmidt, S. Kelly, A.H. Merrill Jr., A. Scherz, Y. Pewzner-Jung, A. Saada, A.H. Futerman, Ablation of ceramide synthase 2 causes chronic oxidative stress due to disruption of the mitochondrial respiratory chain, J. Biol. Chem. 288 (2013) 4947–4956.
[55] S. Orrenius, V. Gogvadze, B. Zhivotovsky, Mitochondrial oxidative stress: implications for cell death, Annu. Rev. Pharmacol. Toxicol. 47 (2007) 143–183.
[56] A. Barrientos, C.T. Moraes, Titrating the effects of mitochondrial complex I impairment in the cell physiology, J. Biol. Chem. 274 (1999) 16188–16197.
[57] V. Geromel, N. Kadhom, I. Cebalos-Picot, O. Ouari, A. Polidori, A. Munnich, A. Rotig, P. Rustin, Superoxide-induced massive apoptosis in cultured skin fibroblasts harboring the neurogenic ataxia retinitis pigmentosa (NARP) mutation in the ATPase-6 gene of the mitochondrial DNA, Hum. Mol. Genet. 10 (2001) 1221–1228.